**Supreet S. Bahga**[1]
**Govind V. Kaigala**[1]
**Moran Bercovici**[2]
**Juan G. Santiago**[1]

[1]Department of Mechanical Engineering, Stanford University, CA, USA
[2]Department of Aeronautics and Astronautics, Stanford University, CA, USA

## Research Article

# High-sensitivity detection using isotachophoresis with variable cross-section geometry

We present a theoretical and experimental study on increasing the sensitivity of ITP assays by varying channel cross-section. We present a simple, unsteady, diffusion-free model for plateau mode ITP in channels with axially varying cross-section. Our model takes into account detailed chemical equilibrium calculations and handles arbitrary variations in channel cross-section. We have validated our model with numerical simulations of a more comprehensive model of ITP. We show that using strongly convergent channels can lead to a large increase in sensitivity and simultaneous reduction in assay time, compared to uniform cross-section channels. We have validated our theoretical predictions with detailed experiments by varying channel geometry and analyte concentrations. We show the effectiveness of using strongly convergent channels by demonstrating indirect fluorescence detection with a sensitivity of 100 nM. We also present simple analytical relations for dependence of zone length and assay time on geometric parameters of strongly convergent channels. Our theoretical analysis and experimental validations provide useful guidelines on optimizing chip geometry for maximum sensitivity under constraints of required assay time, chip area and power supply.

## 1 Introduction

### 1.1 General aspects

Isotachophoresis (ITP) is an electrophoretic separation and preconcentration technique widely applied to food analysis, genetics, pharmacology and toxin detection [1, 2]. In ITP, analytes simultaneously focus and can separate between a high effective mobility leading electrolyte (LE) ions and low effective mobility trailing electrolyte (TE) ions. When present in sufficient amount, the analytes focus and segregate into distinct, contiguous zones with locally uniform (plateau-like) concentrations [3]. However, when analytes are present in trace quantities, they focus into peaks of width determined by the diffusive interface between neighboring zones. These two regimes are respectively termed as "plateau mode" and "peak mode" ITP [4, 5].

Several adjacent analytes in peak mode are practically indistinguishable from each other.

Plateau mode ITP is characterized by locally uniform zone concentrations whose values are governed by the LE buffer characteristics. At the zone boundaries, the analyte ions diffuse into adjacent zones. Assuming negligible advective dispersion [5], the thickness of boundaries is limited by molecular diffusion and decreases at higher electric fields. In ITP separations, plateau mode is often preferred over peak mode as analytes simultaneously preconcentrate and separate distinctly into purified zones. In the case of directly detectable analytes, plateaus can be detected by measuring, for example, electrical conductivity [6] or UV absorption [7]. The displacement physics of plateau mode ITP also enables indirect detection methods including the non-focusing tracer (NFT) technique [8] and the fluorescent mobility markers technique [9, 10]. Typical detected signals in plateau mode ITP are a series of distinct steps in the measured quantity (e.g. as with conductivity [6] or fluorescence intensity [9, 10]). The relative step heights in the signal yield information regarding the electrophoretic mobility of the analytes in respective zones [8]. The width of plateau zones is proportional to the amount of focused analyte, and ability to detect trace analytes is limited by the

**Correspondence:** Professor Juan G. Santiago, 440 Escondido Mall, Bldg. 530, Room 225, Stanford, CA 94305, USA
**E-mail:** juan.santiago@stanford.edu
**Fax:** +1-650-723-7657

**Colour Online:** See the article online to view Figs. 1,3,4 and 6 in colour.

width of plateau zones relative to the width of interfaces. The sensitivity can therefore be expressed as signal-to-noise ratio (SNR) given by the length of the analyte plateau zone normalized by the characteristic length of diffused zone boundaries [9, 10]. Directly opposed to common elution techniques like zone electrophoresis [11], therefore, ITP signals yield resolution information from signal values (and their fluctuations), and sensitivity information from measures of the independent parameter (e.g. time or space).

Several methods have been published to improve the sensitivity of plateau mode ITP. These include (i) using long channels, (ii) application of hydrodynamic counter-flow [12], (iii) using a concentration cascade of LE [13] and (iv) cross-sectional area variation [14, 15]. Techniques such as using longer channel and hydrodynamic counter-flow allow longer time for samples to accumulate prior to detection, thereby attaining larger analyte zone length. However, long (uniform) channels make low voltage operation difficult and counter-flow ITP requires additional off-chip instrumenta-tion for precise control of adverse pressure gradient. Another way to improve sensitivity is by using concentration cascade of ITP [13]; wherein a high-concentration LE is used initially to obtain a large sample accumulation rate, and is followed by a low concentration LE to force longer analyte zones. We estimate that the increase in sensitivity of the latter is therefore limited by the ratio of two LE concentra-tions, which is typically of order 10. This is because the requirements of sufficient solubility and maximum electric field (to avoid Joule heating) impose a limit on maximum LE concentration. Meanwhile very low LE concentrations lead to loss of buffer capacity and robustness of the assay.

An elegant approach to higher sensitivity via variation of the cross-sectional area of the ITP channel was first intro-duced by Everaerts et al. [14]. We depict the concept in Fig. 1. Figure 1B shows a schematic of a channel with varying cross-section. Sample is focused in a large cross-section channel and subsequently detected in a smaller cross-section (high electric field region) channel. Since the mass flux of analyte in ITP is proportional to local cross-section area and system current, large amounts of sample are accumulated in the large cross-section channel. As the analyte zone enters the smaller cross-section channel, the zone elongates to conserve the mass, resulting in improved sensitivity (in comparison to a uniform cross-section chan-nel depicted in Fig. 1A). This technique is also known as column coupling [14] or volume coupling in ITP [15], and is particularly interesting as standard chemistries can be used without pressure-driven flow control. For example, Dolnik et al. [15] used column coupling and a potential gradient (conductivity) detector to detect $1\,\mu M$ concentrations of β-alanine, γ-aminobutyric acid and creatinine as model analytes. Also, Bodor et al. [16] demonstrated on-chip inte-gration of this technique and showed conductivity-based detection of $20\,\mu M$ concentrations of several anions, such as chloride, sulfate, nitrate and phosphate ions. Bodor et al. [16] also demonstrated the use of cross-sectional area variation as a pre-separation step for on-chip coupled ITP-capillary zone
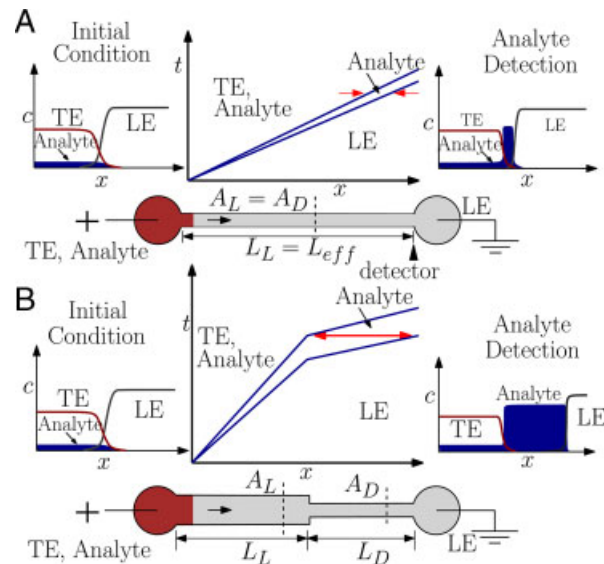


**Figure 1.** Schematic illustrating the effect of varying channel cross-section on sensitivity of isotachophoretic separation and detection. In the channel schematic, the reservoir on the right and the channel are initially filled with LE, and a mixture of TE and analyte is present in the reservoir on the left. Upon application of current, the analyte focuses between the LE and TE zone. (A) For a uniform cross-section channel and constant current, the analyte-to-LE and TE-to-analyte interfaces propagate at constant speeds. The speed of the former is slightly larger than the latter due to the accumulation rate of sample. In the characteristic (space-time) diagram, the propagating interfaces appear as straight lines at different angles to the *x*-axis. (B) shows ITP separation in a channel with variable cross-section areas. The concentration shocks propagate slower in the large cross-section region and faster in the smaller cross-section due to respectively low and high electric fields in these sections. For a finite time, the leading interface of the analyte zone (in the thinner channel) migrates faster than the trailing interface (in the thick section). The varying shock velocities thus result in a rapid expansion of the analyte zone, which proceeds until the TE interface also enters the thinner section.

electrophoresis (ITP-CZE) (where ITP is disrupted to initiate CZE). However, despite its use in such applications, there has been no systematic theoretical and experimental study of the effects of cross-section variation on sensitivity in ITP.

In the current paper, we develop a methodology for designing ITP channels with variable cross-sectional area to achieve plateau mode and improve sensitivity to detect trace analytes. We consider constraints on geometry, detection time and applied voltage (or current). Understanding the tradeoffs between various figures of merit and developing appropriate design tools is especially important for on-chip systems with either limited chip area or limited voltage, such as portable ITP systems [17]. We begin by presenting a new formulation for ITP dynamics which leverages a diffusion-free model for fast calculations and which is particularly useful in plateau mode ITP problems in variable cross-section channels. We present comparisons of the model with more comprehensive numerical predictions. More importantly, we present extensive validation of the model using a series of controlled experiments on a set of microfluidic chips with varying geometries. We then leverage

our model to derive a set of algebraic relations for the dependence of zone length and assay time on channel geometry. In particular, the model elucidates the advantage of using variable cross-section geometries, to reduce assay time (compared to the assay time in uniform cross-section channels) for a given SNR. Finally, using a channel with a cross-section area ratio of 16, we demonstrate indirect fluorescence detection with a sensitivity of 100 nM. To the best of our knowledge this is the most sensitive demonstration of indirect detection on chip.

## 1.2 Theory

Several models exist with varying degrees of complexity that approximate the physics of ITP. Most basic analytical models of ITP are based on describing purified (i.e. a single co-ionic species within each zone) plateau-mode properties at steady state. Under these conditions, and for finite amounts of sample, all interfaces in ITP travel at equal velocities. For fully ionized species, the statement of conservation of charge and continuity of current describing these problems is Kohlraush's law [19]. Conservation principles based on electroneutrality and current continuity for weak electrolytes are the Jovin and Alberty's relations [20, 21]. The Kohlrausch function is applicable for strong, multivalent electrolyte systems, and the Jovin and Alberty functions apply to weak, univalent electrolyte systems. However, none of these simple models describe unsteady dynamics of ITP (e.g. startup, development phase). We also note that latter two functions do not strictly apply to the case where sample analytes are mixed uniformly with the TE (semi-infinite injection) [22], or when hydronium and hydroxide ion concentrations are comparable to electrolyte concentrations. In the latter case where the TE-analyte mixture yields a steady supply of analytes, true steady state is never obtained and sample zones grow slowly in time as ITP progresses and so interfaces move at different velocities. Thus, unsteady models are required for such processes.

One approach for unsteady ITP problems is full numerical simulations of one-dimensional (1-D) area averaged advection–diffusion transport equations [23–26]. Such simulations are complex and typically limited to channels with uniform cross-section. Hruška et al. [27] presented results from a modified version of their Simul simulation program [24] to analyze an isoelectric trapping in a system, which couples channels of different cross-sectional areas (each channel with a uniform cross-sectional area). However, the latter work provides no description of the numerical implementation to handle coupled channel areas. Also, all simulations of 1-D area averaged advection–diffusion equations [23–27] are significantly more time consuming than the diffusion-free approximation presented here. Further, semi-analytical approaches such as that described here offer physical insights into problems and can point out key parameters and figures of merit.

The assumption of negligible diffusion often holds well for plateau mode ITP, as diffusion effects are often limited to interface regions, which are typically small compared to zone lengths. For example, Zhukov [28] developed a detailed unsteady diffusion-free model for ITP. A key limitation to Zhukov's model is the assumption of analytes to be fully ionized or very weakly ionized (negligible degree of ionization). Zusková et al. [29] presented a diffusion-free formulation for modeling unsteady ITP in the presence of a single a common component (admixture) in LE and TE. The latter model applies to both strong and weak electrolytes. However the models by Zhukov [28] and Zusková et al. [29] apply only to channels with uniform cross-sections. In fact, to the best of our knowledge, all ITP models to date (e.g. [19–21, 23–29]) cannot handle a general variation in channel cross-section (and the extended Simul [27] results presented for isoelectric focusing handle piecewise constant cross-sections only).

Below, we present a model that focuses on unsteady ITP separation dynamics in variable cross-section channels. The model is well suited for unsteady and steady state plateau mode ITP problems and can handle both an arbitrary number of weak or strong electrolytes and varying cross-sectional area channels.

## 1.3 Diffusion-free model

We start with electromigration-diffusion transport equation,

$$\frac{\partial c_i}{\partial t} = \nabla \cdot (\mu_i c_i \nabla \phi + \nabla(D_i c_i)), \quad i = 1, \ldots, N, \quad (1)$$

where $c_i$, $\mu_i$ and $D_i$ denote the concentration, effective mobility and molecular diffusivity of species $i$, and $\nabla \phi$ is the electric field. We here define mobility as a signed quantity $\mu_i = u_i / E$ where $\mu_i$ is species drift velocity and $E$ is local electric field. Evaluating Eq. (1) in one dimension, integrating over the cross-section, neglecting diffusion, and using $\nabla \phi = -J/(A(x)\sigma)$ we obtain,

$$\frac{\partial c_i}{\partial t} + \frac{J}{A(x)} \frac{\partial}{\partial x} \left( \frac{\mu_i c_i}{\sigma} \right) = 0, \quad \sigma = \sum_{i=1}^{N} z_i \mu_i c_i F. \quad (2)$$

where $\sigma$ is the electrical conductivity and $J$ is current through the separation channel. $A(x)$ is the cross-sectional area of the channel allowed to vary over the axial channel dimension $x$. Equation (2) can be further simplified by transforming the spatial coordinate $x$ to a volume coordinate $\eta$,

$$\frac{\partial c_i}{\partial t} + J \frac{\partial}{\partial \eta} \left( \frac{\mu_i c_i}{\sigma} \right) = 0, \quad \eta = \int_0^x A(\xi) \, \mathrm{d}\xi \quad (3)$$

The above equation is similar to 1-D transport equation without diffusion, except it is now based on a new (volume) coordinate $\eta$ instead of $x$. Integrating Eq. (3) over a small element $(\eta, \eta + \mathrm{d}\eta) \times (t, t + \mathrm{d}t)$ around a shock we obtain the Hugoniot jump conditions [30] across that shock,

$$\int_t^{t+\mathrm{d}t} \int_\eta^{t+\mathrm{d}\eta} \left( \frac{\partial c_i}{\partial t} + J \frac{\partial}{\partial \eta} \left( \frac{\mu_i c_i}{\sigma} \right) \right) \mathrm{d}\eta \mathrm{d}t = 0,$$

$$\frac{\mathrm{d}x}{\mathrm{d}t} (c_i^+ - c_i^-) = \frac{J}{A(x)} \left( \frac{\mu_i^+ c_i^+}{\sigma^+} - \frac{\mu_i^- c_i^-}{\sigma^-} \right). \quad (4)$$

where $-$ and $+$ denote the evaluation of a property behind and in front of a shock, respectively. Solving for these jump conditions across each shock and for each species, we obtain the concentrations and shock speeds ($dx/dt$). We present a more detailed formulation of this problem in the Supporting Information. In a system consisting of simply LE ions, terminating electrolyte ions, and analyte and background counter-ion; two propagating shocks form. These correspond to the adjusted-TE-to-analyte interface and the analyte-to-LE interface, as shown in Fig. 1. The "adjusted TE" refers to the trailing electrolyte co-ion region now occupying the region vacated by the LE (and therefore matching the Jovin and Alberty functions [20, 21] set by the LE). The properties of the adjusted TE are independent of the initial concentration of TE and set by the LE. We will refer to the initial properties of the TE as those of the "TE well". The adjusted TE-to-analyte interface propagates at speed, $\mu_{t,T}J/(\sigma_T A)$, while the speed of analyte-to-LE interface is given by $\mu_{l,L}J/(\sigma_L A)$. Here, $\mu_{t,T}$ and $\mu_{l,L}$ are the effective mobilities [31] of TE ions in the adjusted TE zone and LE ions in the LE zone, respectively, while $\sigma_T$ and $\sigma_L$ denote the conductivity of adjusted TE and LE zones. (In our notation, the first small-case subscript identifies the ion, and the second capitalized subscript identifies the zone of interest.)

Let $x(t)$, $y(t)$ and $z(t)$ denote the coordinates of the analyte-to-LE, adjusted TE-to-analyte, and the TE well-adjusted TE interfaces, respectively. We can account for possible electroosmotic flow (EOF) in the channel by subtracting the local bulk velocity of $\bar{Q}_{EOF}/A(x)$ to the velocity of the interfaces in the channel. Thus, the time evolution of these interfaces can be written in form of a set of ordinary differential equations,

$$\text{analyte-to-LE}: \frac{dx}{dt} = \frac{\mu_{l,L}J}{\sigma_L A(x)} + \frac{\bar{Q}_{EOF}}{A(x)}, \quad x(0) = 0$$

$$\text{adjusted TE-to-analyte}: \frac{dy}{dt} = \frac{\mu_{t,T}J}{\sigma_T A(y)} + \frac{\bar{Q}_{EOF}}{A(y)}, \quad y(0) = 0$$

$$\text{TE well-to-adjusted TE}: \frac{dz}{dt} = \frac{\bar{Q}_{EOF}}{A(z)}, \quad z(0) = 0$$

$$(5)$$

where $\bar{Q}_{EOF}$ is the mean flow rate due to the product of electric field and EOF mobility averaged over the length of the channel. See Ghosal [32], and Bhardwaj and Santiago [33] for similar treatments of EOF in area-averaged channels. The system of ordinary differential equations Eq. (5) is coupled because $\bar{Q}_{EOF}$ depends on the location of all shocks. Each zone has an associated local electric field that couples with local EOF mobility to contribute to overall bulk flow. Also, for a constant applied voltage across the channel, the current, $J$, depends on location of all interfaces, as the channel resistance changes with time.

The zone length, $\Delta_P$, of focused analyte is given by the difference between positions of analyte-to-LE interface and the adjusted TE-to-analyte interface, $\Delta_P(t) = x(t) - y(t)$. Solution to Eq. (5) is obtained by numerical integration. Figure 2 shows a comparison of our model with a full 1-D

simulation using SPRESSO [25, 26] for the case of buffering (weak electrolyte) counter-ion, a strong electrolyte LE, a weak acid analyte, and a weak acid TE (see figure caption for details). The comparison with the full SPRESSO simulation (which includes diffusion) shows excellent agreement in zone concentrations and zone length. As shown in the figure, the effects of diffusion are limited to zone boundaries in this plateau mode ITP problem. We emphasize that even the final time solution shown cannot be obtained using steady state models (e.g. similar to that of Everaerts et al. [18]) as such models apply conservation laws assuming that all shocks are propagating at equal speeds. We also note that, even in the case where diffusion length scales are significant relative to (or larger than theoretical) zone lengths, the current diffusion-free model will yield the correct amount of sample accumulated in each analyte zone. For example, if the sample is physically accumulated in peak mode, the current model will yield a short theoretical plateau zone, which contains the correct amount of accumulated analyte.
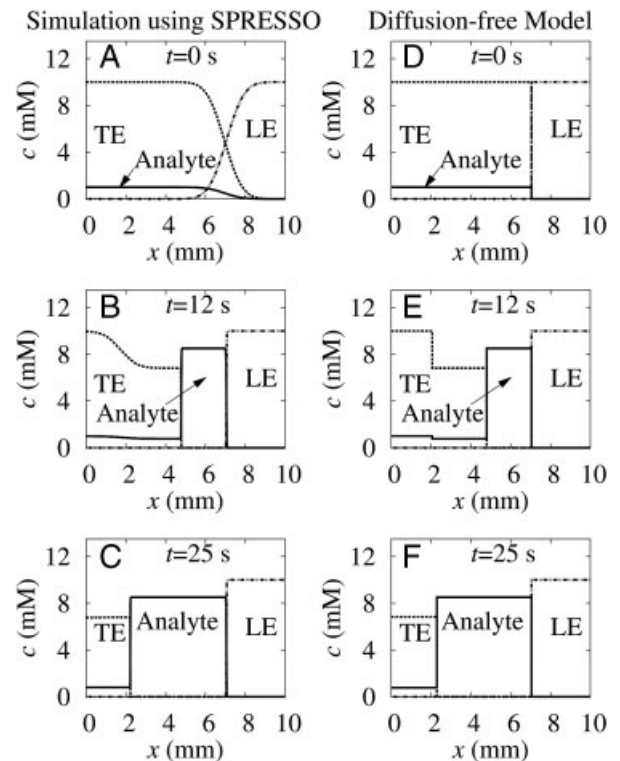


**Figure 2.** Comparison of our diffusion-free model (D–F) with a full numerical simulation (A–C), for the case of plateau mode ITP with semi-infinite injection of analyte (i.e. analyte mixed homogenously with TE). Simulations for detailed electromigration-diffusion model were performed using our open source code Spresso [25, 26]. The numerical calculations were performed in a frame of reference moving with the LE-analyte interface. The diffusion-free model predicts plateau zone lengths correctly as diffusion effects are limited to zone boundaries. LE is 10 mM HCl and 20 mM Bistris; TE is 10 mM Tricine and 20 mM Bistris; and the model analyte is 1 mM acetic acid. Calculations were performed for a constant current of 1 μA, applied through a circular channel with uniform cross-section of diameter 50 μm.

## 1.4 Analytical relations and scaling arguments for varying cross-sectional area channels

We use the model presented in Section 1.3 to derive analytical relations for the dependence of plateau zone length and detection time on channel geometry and buffer chemistry. Consider the separation channel in Fig. 1B, consisting of a large cross-section region with area $A_L$, followed by a smaller cross-section region with area $A_D$. In ITP with semi-infinite injection, the analyte primarily accumulates in the large cross-section channel, which we refer to as the "loading section." This accumulation is often in peak mode. The analyte zone then reaches the small cross-section channel and expands axially along the channel, resulting in a newly created plateau or plateau with larger zone length. To achieve higher sensitivity, the analyte is detected in this smaller cross-section channel, which we will refer to as the "detection section." The zone length, $\Delta_P$, is obtained by solving Eq. (5). Assuming negligible EOF, Eq. (5) can be written as,

$$\frac{\mathrm{d}\gamma}{\mathrm{d}x} = \frac{\mu_{t,T}\sigma_L}{\mu_{l,L}\sigma_T}\frac{A(x)}{A(\gamma)}, \tag{6}$$

which describes the relative motion of the trailing interface to the leading interface. For a varying cross-section channel with large cross-section followed by small cross-section region (each section with uniform area) as in Fig. 1B, Eq. (6) can be solved to obtain,

$$\int_0^{L_L} A(\gamma)\,\mathrm{d}\gamma = \frac{\mu_{t,T}\sigma_L}{\mu_{l,L}\sigma_T}\int_0^{L_L+\Delta_P} A(x)\,\mathrm{d}x$$

$$A_L L_L = \frac{\mu_{t,T}\sigma_L}{\mu_{l,L}\sigma_T}(A_L L_L + A_D \Delta_P) \tag{7}$$

Rearranging this expression, we obtain an expression for zone length, $\Delta_P$, in terms of channel geometry and electrolyte chemistry,

$$\Delta_P = \left(\frac{\mu_{l,L}}{\sigma_L} - \frac{\mu_{t,T}}{\sigma_T}\right)\left(\frac{A_L L_L}{A_D}\right)\frac{\sigma_T}{\mu_{t,T}}. \tag{8}$$

Next, we apply the jump conditions (4) across the TE-to-analyte interface and define $V_{\mathrm{ITP}} = \mu_{a,A}J/\sigma_A = \mu_{l,L}J/\sigma_L$, where $V_{\mathrm{ITP}}$ is the velocity of the LE-to-analyte interface. Thus, the parenthetic mobility term on the right-hand-side of (8) can be written explicitly in terms of analyte concentrations:

$$\left(\frac{\mu_{l,L}}{\sigma_L} - \frac{\mu_{t,T}}{\sigma_T}\right) = (\mu_{a,T} - \mu_{t,T})\frac{c_{a,T}}{\sigma_T c_{a,A}} \tag{9}$$

The concentration of analyte in the adjusted TE zone, $c_{a,T}$, can then be related to its concentration in the well using the jump conditions across the stationary interface of TE well and adjusted TE,

$$\frac{\mu_a^0}{\sigma^0}c_a^0 = \frac{\mu_{a,T}}{\sigma_T}c_{a,T}. \tag{10}$$

where the superscript describes a property evaluated at the well. Combining expressions (8)–(10) we obtain an explicit

dependence of zone length on the concentration of the analyte in the TE well and on channel geometry,

$$\Delta_P = \left(1 - \frac{\mu_{t,T}}{\mu_{a,T}}\right)\frac{\mu_a^0}{\mu_{t,T}}\frac{\sigma_T}{\sigma^0}\left(\frac{A_L L_L}{A_D}\right)\frac{c_a^0}{c_{a,A}}. \tag{11}$$

This shows that the plateau zone length of an analyte, $\Delta_P$, is proportional to both the concentration of the analyte in the well, $c_a^0$, and to the geometric parameter $A_L L_L/A_D$. This geometric parameter is equivalent to the total length of a uniform cross-section channel (irrespective of cross-sectional area or applied current), which would have been required to obtain the same zone length. We therefore refer to $A_L L_L/A_D$ as the "effective length" of the variable-area channel, and denote it by $L_{eff}$. For a given chemistry, the zone length, $\Delta_P$ therefore scales as,

$$\Delta_P \propto L_{eff}c_a^0, \qquad L_{eff} = \frac{A_L L_L}{A_D}. \tag{12}$$

Resource limits on applied voltage and/or applied current influence the dynamics since they directly affect the detection time. For example, the miniaturized ITP device of [10] had a voltage limited to 200 V (currently, this device has a limit of 350 V). To derive an appropriate scaling for the detection time in such systems, we here neglect EOF, and solve for the location of the front interface with Eq. (5),

$$\frac{\mathrm{d}t}{\mathrm{d}x} = \frac{\sigma_L A(x)}{\mu_{l,L}}\frac{\Delta V}{R(x)}. \tag{13}$$

Here $R$ denotes the electrical resistance of the channel. The resistance of the channel increases during ITP, as high-conductivity LE is replaced by a lower conductivity TE. Since the analyte zone is typically much smaller than the overall channel length, we here neglect its contribution to the channel resistance. With this assumption we show in the Supporting Information that the detection time, $T$, can be approximated as

$$T \approx \frac{L_L L_D}{\mu_{l,L}\Delta V}\left(\frac{A_L}{A_D} + \frac{1}{2}\left(1 + \frac{\sigma_L}{\sigma_T}\right)\frac{L_L}{L_D}\right). \tag{14}$$

The two analytical expressions (12) and (14) enable simple evaluation of the advantages of using variable cross-section channels over uniform cross-section channels. For example, if we take $A_L/A_D = 10$, $L_L = L_D = L$, $\sigma_L/\sigma_T = 10$, then from Eq. (12) the effective length is $L_{eff} = 10L$. This means that in order to obtain same zone length, a uniform cross-section channel would require a 10-fold longer channel. Furthermore, using Eq. (14), one can show that the detection time using the variable cross-section geometry is 35-fold shorter than that of a longer channel with uniform cross-section and actual length equal to $L_{eff}$ ($L_L = L_{eff}$, $L_D = 0$). This example shows that variable cross-section channels not only results in higher sensitivity compared to fixed cross-section channels, but also in significantly shorter detection times for fixed plateau widths.

Theoretical plateau widths are directly relevant to sensitivity of the assay. For example, a good working definition for the sensitivity limit is when the theoretical plateau width is significantly larger (say twice or more) than the

interface width caused by diffusion and advective dispersion (see Khurana and Santiago [9] for further discussion). Plateau zone lengths are independent of applied voltage or current (see Eq. 11). However, in the absence of advective dispersion [9], interface thickness is inversely proportional to the electric field in the channel [23]. Thus, the interface thickness (and SNR) show different dependence on channel geometry for constant voltage and constant current operation.

The trade-offs of assay time, SNR, channel area ratio, applied voltage and applied current are discussed in detail in the Supporting Information, and summarized here. For fixed voltage operation, increasing cross-section ratio results in larger zone length, higher electric field and sharper interfaces. Therefore, SNR improves significantly by increasing the cross-section ratio. Whereas, increasing length of the loading section increases the zone length but leads to lower electric field and thicker interfaces. Thus, SNR does not improve significantly by increasing the length of loading section. For a fixed voltage and channel length, SNR can be increased by increasing the cross-sectional area ratio, but at the expense of longer assay time.

In contrast, for fixed current operation, electric field and interface thickness in the detection section do not depend on the dimensions of the loading section. Therefore, significant improvements in SNR can be obtained by increasing both cross-section ratio and loading length, which give larger zones and sharper zone boundaries. For both fixed current and channel length, SNR can be increased by decreasing the area of detection section ($A_D$), without increasing the assay time.

## 2 Materials and methods

We performed a series of experiments with varying channel geometries and analyte concentrations to validate our model. We performed cationic ITP experiments to avoid interference of bicarbonate ions (from reaction of dissolved carbon dioxide with water), which can focus and create spurious analyte zones [34, 35]. For these cationic ITP validation experiments, the LE ion was the sodium ion from 10 mM NaOH, TE ion was 10 mM Pyridine, and 20 mM Hepes was used as the counter-ion. To study the effect of analyte concentration we varied the model analyte (Bistris) concentration from 1 to 4 μM. We also prepared 1 mM stock solution of the Alexa-Fluor 488 dye (Invitrogen, Carlsbad, CA), and used it to visualize the plateau zones of cationic ITP as an NFT ion [8] by mixing at a concentration of 70 μM in the LE. For the experiments demonstrating 100 nM sensitivity, we used the same buffer ions but reduced TE concentration to 3 mM Pyridine with 6 mM Hepes to increase electric field and focusing rate.

For the experiments demonstrating the principle of the variable cross-section technique (see Fig. 3) we used 50 mM NaOH and 100 mM Hepes as LE buffer; 10 mM Pyridine and 20 mM Hepes as TE buffer. We used 10 μM Bistris as the model focusing analyte, initially mixed with TE.

For all experiments presented in this paper, we added respectively 1 and 0.5% polyvinylpyrrolidone (PVP) to LE and the TE to suppress EOF. All chemicals were obtained from Sigma Aldrich (St. Louis, MO) and diluted from 1 M stock solutions. All solutions were prepared in UltraPure DNase/RNase free distilled water (GIBCO Invitrogen).

We captured images using an inverted epifluorescent microscope (IX70, Olympus, Hauppauge, NY) equipped with a LED lamp (LEDC1, Thor Labs, Newton, NJ), U-MWIBA filter-cube from Olympus (460–490 nm excitation, 515 nm emission, and 505 nm cut off dichroic) and a 10× (NA = 0.4) UPlanApo objective (Olympus). Images were captured using a 12 bit, 1300 × 1030 pixel array CCD camera (Micromax1300, Princeton Instruments, Trenton, NJ). We controlled the camera using Winview32 (Princeton Instruments) and processed the images with MATLAB (R2007b, Mathworks, Natick, MA). We conducted the experiments by applying constant voltage across the micro-channels using a sourcemeter (model 2410, Keithley Instruments, Cleveland, OH).

All experiments were performed on custom-made, wet-etched, borosilicate glass microfluidic chips fabricated
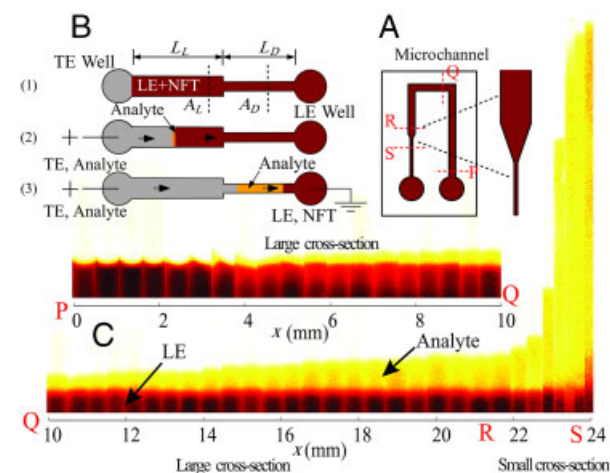


**Figure 3.** ITP injection protocol and variation of analyte zone length along the separation channel. (A) Glass microchips consisted of a large cross-sectional area loading section (sections P, Q and R) of length $L_L$ and then a smaller cross-section detection section (detector at S) of length $L_D$ (see Table 1). (B) Channel schematic showing ITP with semi-infinite analyte injection: (1) We filled the LE well with a mixture of LE and NFT and applied vacuum on TE well. We then emptied the TE well, rinsed, and filled it with a mixture of analyte and TE, and (2) applied potential between the TE and LE reservoirs. The NFT concentration adjusted to the local electric field and we imaged the steps in fluorescent intensity. (3) the analyte zone expanded in the small cross-section. (C) shows 49 raw inverted-fluorescent intensity images of the analyte zone as a function of axial position along the channel, x. The analyte zone length grows slowly while in the large cross-section region, and then rapidly elongates as it enters the small cross-section region ($x > 22$ mm). For the images, we used a constant applied potential of 700 V on a chip with large and small cross-sections of 1450 and 90 μm², respectively. We here subtracted the mean value of intensity in TE zone for clarity of presentation.

using standard lithographic processes. Figure 3A shows a schematic of the microfluidic chips, consisting of a single channel with end-channel reservoirs (2 mm holes diamond-drilled into cover glass of chip). The channels consisted of sections with relatively large (1400–2230 $\mu m^2$) cross-sectional areas followed by section with a 90–1400 $\mu m^2$ cross-section. The geometric parameters of all channels used in this study are listed in Table 1. All experiments used a semi-infinite injection scheme wherein the analyte was initially mixed with TE. We visualize ITP zones by indirect fluorescence detection using an NFT technique [8] (see Section 3). Figure 3B shows the ITP assay protocol for our ITP experiments. We filled the East well of the chip with a mixture of LE and NFT and applied vacuum to the West well until the channel was filled. We then rinsed the West well several times with deionized water and filled it with the mixture of TE and analyte. The electrodes were placed in the East and West wells and constant voltage was applied. We centered the field of view of the microscope at a fixed distance of 1 mm to the right of the junction of the large and small area channel sections, and set the camera to obtain images continuously until manually stopped after capturing images of ITP zones.

## 3 Experiments

We performed experiments to validate the diffusion-free, variable area ITP dynamics model and study the effects of area variation on analyte detection sensitivity via ITP.

### 3.1 Parametric variations and zone visualizations

To validate the model presented in Section 1.3, we conducted a detailed parametric study in which we varied analyte concentrations in the range 1–4 $\mu M$, and varied chip geometries to vary effective lengths from 10 to 241 mm (see Table 1). We implemented NFT using an anionic fluorescent species mixed with LE. In cationic ITP, fluorescent anions do not focus, but their concentration adjusts to the local electric fields in different zones. Using mass flux balance across the analyte-to-LE interface, Chambers and Santiago [8] showed that the concentration of non-focusing

tracer in analyte zone is given by

$$\frac{c_{NFT,A}}{c_{NFT,L}} = \frac{\mu_{a,A}}{\mu_{l,L}} \left( \frac{\mu_{NFT,L} - \mu_{l,L}}{\mu_{NFT,A} - \mu_{a,A}} \right) \tag{15}$$

where $\mu_{NFT}$ denotes the effective mobility of (here, anionic) NFT. The step change in concentration of NFT is observed as a step change in fluorescence signal. Figure 3C shows NFT visualization of analyte zone along a variable cross-section channel. The inverted intensity images (high intensity implies high NFT concentration and low local electric field) in Fig. 3C show the analyte zone slowly increasing in length in the loading (larger cross-section) section. As the analyte zone enters the detection section, it spreads out, the zone length increases and the zone boundaries sharpen due to higher local electric field.

### 3.2 Effect of initial analyte concentration on zone length

We performed experiments to validate the dependence of zone length on initial concentration as given by Eq. (12). For this effect, we varied analyte concentration while keeping the channel geometry fixed. We used Channel 4 (see Table 1) and varied the concentration of the analyte from 1 to 4 $\mu M$. Figure 4 shows the variation of measured and theoretical zone lengths, as a function of the concentration of the analyte in the well. We observed a proportional increase in zone length with analyte concentration. This is expected as the flux of analyte into the analyte zone is proportional to the concentration of analyte in the TE well (i.e. the concentration in the unadjusted TE).

Although we suppressed EOF using PVP, we observed residual EOF in our experiments. We accounted for EOF as follows. As ITP progresses, the lower conductivity analyte and TE mixture replaces higher conductivity LE in the channel, resulting in increased resistance and lower overall current. We observed only gradual decrease in current with time while the TE was in the loading section, as expected. When the TE zone entered the detection section, resistance increased rapidly and we observed a sudden drop in current. We accounted for EOF by tuning a (uniform) EOF mobility in our model so as to

**Table 1.** Geometric parameters of the five microchannel geometries used in this study

| Chip no. | Thicker loading section | | Thinner detection section | | Effective length $L_{eff}$ (mm) |
|---|---|---|---|---|---|
| | Area $A_L$ ($\mu m^2$) | Length $L_L$ (mm) | Area $A_D$ ($\mu m^2$) | Length $L_D$ (mm) | |
| 1 | 1400 | 10 | 1400 | 7.5 | 10 |
| 2 | 2000 | 5 | 90 | 7.5 | 111 |
| 3 | 1500 | 10 | 90 | 7.5 | 167 |
| 4 | 2230 | 10 | 90 | 7.5 | 241 |
| 5 | 1450 | 22 | 90 | 8.0 | 354 |

The effective length is defined as $L_{eff} = A_L L_L / A_D$.
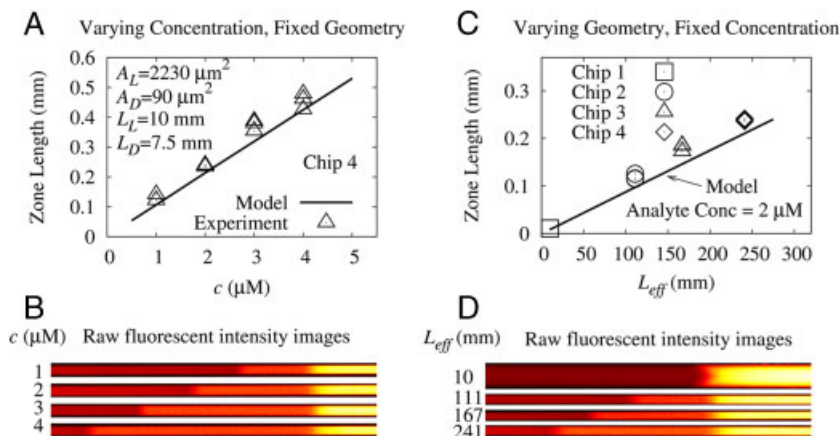
**Figure 4.** Effect of analyte concentration and channel geometry on zone length. (A) shows the variation of measured and theoretical zone length as a function of analyte concentration in the chip TE well and for a fixed chip geometry (Chip ♯4 of Table 1). Theoretical predictions are in good agreement with experimental observations. (B) shows corresponding example images for four concentrations. (C) shows measured and predicted values of analyte zone length for as a function of effective channel lengths, $L_{eff} = A_L L_L / A_D$ (representing four channel geometries) and a fixed analyte concentration of 2 μM. (D) shows the corresponding experimental images. The top image in (D) shows the case for the uniform area channel, $L_L = L_{eff} = 10$ mm, where no analyte plateau was observed as analyte is in peak mode. However, the images below that show that the same analyte concentration and applied voltage yields significant increase in sensitivity (plateau zone length) for increased effective lengths associated with the area ratios of Chips 1–4 of Table 1. All data here are for 350 V applied voltage, and the NFT is 70 μM AlexaFluor-488. EOF mobility is $2 \times 10^{-9}\,\mathrm{m^2\,V^{-1}\,s^{-1}}$.

match the observed time at which the TE enters the detection section. This yielded an estimate EOF mobility of $2 \times 10^{-9}\,\mathrm{m^2\,V^{-1}\,s^{-1}}$. The model uses this simple empirical estimate of residual EOF to estimate zone length as a function of position as shown in Fig. 4A.

Figure 4A shows measurements of zone length as a function of analyte concentration for Chip 4 of Table 1, as well as corresponding image data (flat-field corrected, raw images) for these experiments. As shown, the model agrees very well with measurements of analyte zone length versus initial analyte concentrations.

### 3.3 Effect of channel geometry on zone length

We also experimentally established the effect of channel geometry on zone length. We performed ITP experiments on four chip geometries with effective lengths, $L_{eff}$, ranging from 10 to 241 mm, and using an identical analyte concentration of 2 μM and applied voltage of 350 V. As shown in Table 1, the changes in effective length were obtained by changing both the cross-sectional area ratios and the lengths of the loading zone. Figure 4C shows the dependence of measured zone length on effective length of the channel. The experiments show the zone length to be directly proportional to the effective length, as predicted by our theoretical model.

We note that for a uniform cross-section channel with $L_{eff} = L_L = 10$ mm (top image in Figure 4D) we do not observe a plateau, as the analyte is in peak mode. However, the same concentration of analyte and same applied voltage of 350 V yield increasing analyte plateau lengths for chip geometries with longer effective lengths. This illustrates the efficacy of variable cross-section geometries in increasing
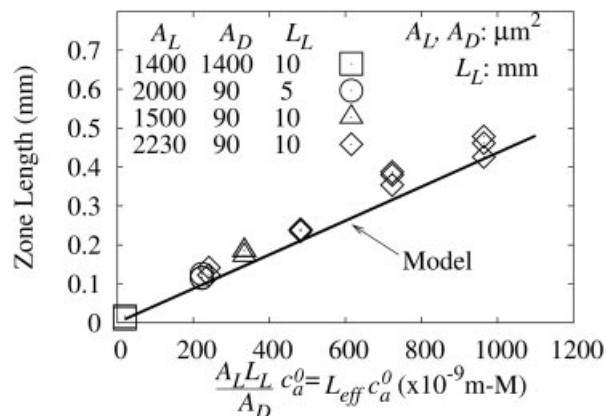


**Figure 5.** Comparison of measured zone length for different geometries and analyte concentration with theoretical scaling of $\Delta_P \propto A_L L_L / A_D c_a^0$. Data points show results presented in Fig. 4, plotted against $L_{eff} c_a^0 = A_L L_L / A_D c_a^0$. Zone length increases linearly with $L_{eff} c_a^0$ for a given choice of LE and TE chemistry. The experimental conditions are similar to those for experiments presented in Fig. 4.

detection sensitivity of ITP. We also emphasize this improvement in sensitivity using variable cross-section geometry compared to uniform cross-section geometry does involve longer detection time. However, as noted in Section 1.4, for the same sensitivity, the detection time using variable cross-section geometry is shorter than the detection time in a uniform cross-section channel.

In Fig. 5, we plot all of the experimental results shown in Fig. 4A and C in a single plot of dimensional zone thickness versus the product $L_{eff} c_a^0$. $L_{eff}$ is the effective length across all chip geometries of the data (Chips 1–4 of Table 1). $c_a^0$ is the analyte concentration in TE well set by the initial

condition (i.e. the analyte level established by a particular application). As predicted by the theory, the analyte plateau length is directly proportional $L_{eff}c_a^0$ and all experimental data points collapse on a single line.

### 3.4 Demonstration of high-sensitivity ITP indirect detection

Lastly, we used a variable cross-section geometry to demonstrate improvement on the sensitivity of an ITP detection with fixed physical length and constant applied voltage. We note that increasing analyte theoretical plateau length, and therefore sensitivity, using variable cross-section channels is independent of the detection technique, direct or indirect. For these experiments we used Chip 5 of Table 1 with effective length of 354 mm but an actual channel length of 30 mm. We were successfully able to detect 100 nM Bistris in 5 min using NFT technique. Figure 6 shows the fluorescent intensity signals corresponding to the control experiment (without analyte), and for 100 and 50 nM Bistris concentrations (for our purposes we here use Bistris model analyte with well-known properties for these controlled experiments). At 100 nM concentration, the Bistris zone is sufficiently resolved. At 50 nM concentration, the Bistris zone plateau length is approximately equal to the
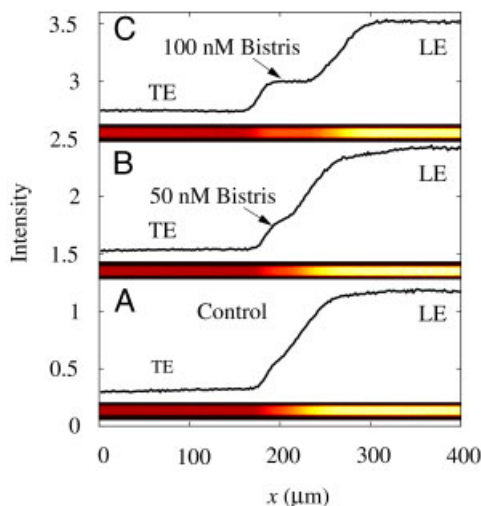


**Figure 6.** Indirect fluorescence detection of 100 nM Bistris using NFT technique with variable area geometry channel. (A) shows a single step in fluorescent intensity, corresponding to the LE and TE zones. (C) shows a distinct step in NFT signal when 100 nM Bistris is mixed with TE. This step corresponds to Bistris focused in plateau mode. (B) shows detection of 50 nM Bistris, initially mixed with TE. For 50 nM concentration, Bistris zone is not distinct enough in comparison with the control signal. This lower SNR at 50 nM Bistris is due to diffusion length scale comparable to the analyte zone thickness. The NFT is 70 μM Alexa-Fluor-488, mixed initially with LE. For these experiments we used a constant potential of 350 V on a chip with effective length of 354 mm, and large and small cross-sections of 1450 and 90 μm², respectively.

length scale of the adjusted TE-to-LE interface, rendering it practically indistinguishable from the control signal.

## 4 Concluding remarks

We have developed a methodology for designing channels with variable cross-sectional area to maximize sensitivity while reducing or minimizing assay time. Our analysis is based on a diffusion-free model of unsteady dynamics of ITP in channels with axially varying cross-section. The model incorporates multispecies electromigration physics. We benchmarked our model with numerical simulations based on an experimentally validated, detailed model of ITP. To verify accuracy in predicting zone lengths, we performed a series of experiments on channels with variable cross-section. Our model predicts and experiments confirm that ITP in initially large and then small cross-sectional area channels leads to higher sensitivity than equal total length channels with uniform cross-section. The large channel cross-section (area $A_L$, where $L$ is for loading) focuses large amounts of sample, and then analyte zones elongate and zone boundaries sharpen in the small cross-section, detection section region (area $A_D$) where electric field is high. For a given buffer chemistry, zone length in the small cross-section channel is directly proportional to initial analyte concentration and an effective length $L_{eff}$ of the channel equal to $L_{eff} = A_L L_L / A_D$, where $L_L$ is the length of the loading section.

We used the diffusion-free model to derive analytical relations for the dependence of zone length and assay time on channel geometry. Based on these relations, we showed that short channels with variable cross-section geometry yield sensitivity comparable to that achieved in much longer channels with uniform cross-section. For fixed voltage and SNR of plateaus, variable cross-section channels reduce both overall channel length and assay time compared to uniform cross-section channels. Further, for fixed voltage and channel length, larger cross-section ratio channels yield better SNR, but at the expense of longer assay time. In contrast, for fixed current operation, SNR can be increased by reducing cross-section of detection section and without increasing the assay time. We presented detailed comparisons of the galvanostatic versus potentiostatic cases in the Supporting Information.

Variation of ITP channel cross-sectional area represents a method of increasing sensitivity in a wide variety of ITP assays, and the approach is relatively independent of the detection method (e.g. applicable to both direct and indirect analyte detection strategies). Our model can be applied for practical use in designing optimal channels, with constraints on SNR, geometry, voltage and detection time. This is particularly important in the context of portable, on-chip systems, with limited voltage supply and chip area. To demonstrate this, we here presented on-chip, indirect fluorescence detection with 100 nM sensitivity using a variable cross-section geometry. The latter is to our

knowledge the highest ever reported sensitivity for ITP in indirect detection mode.

## 5  References

[1] Auroux, P., Iossifidis, D., Reyes, D. R., Manz, A., *Anal. Chem.* 2002, *74*, 2637–2652.

[2] Chen, L. J. E., Fielden, P. R., Goddard, N. J., Manz, A., Day, P. J. R., *Lab Chip* 2006, *6*, 474–487.

[3] Martin, A. J. P., Everaerts, F. M., *Anal. Chim. Acta* 1967, *38*, 233–237.

[4] Chen, S., Graves, S. W., Lee, M. L., *J. Microcol. Sep.* 1999, *11*, 341–345.

[5] Khurana, T. K., Santiago, J. G., *Anal. Chem.* 2008, *80*, 6300–6307.

[6] Zemann, A. J., Schnell, E., Volgger, D., Bonn, G. K., *Anal. Chem.* 1998, *70*, 563–567.

[7] Ludwig, M., Kohler, F., Belder, D., *Electrophoresis* 2003, *24*, 3233–3238.

[8] Chambers, D., Santiago, J. G., *Anal. Chem.* 2009, *81*, 3022–3028.

[9] Khurana, T. K., Santiago, J. G., *Anal. Chem.* 2008, *80*, 279–286.

[10] Bercovici, M., Kaigala, G. V., Backhouse, C. J., Santiago, J. G., *Anal. Chem.* 2010, *82*, 1858–1866.

[11] Jorgenson, J. W., *Trends Analyt. Chem.* 1984, *3*, 51–54.

[12] Everaerts, F. M., Vacik, J., Verheggen, Th. P. E. M., Zuska, J., *J. Chromatogr.* 1970, *49*, 262–268.

[13] Bocek, P., Deml, M., Janak, J., *J. Chromatogr.* 1978, *156*, 323–326.

[14] Everaerts, F. M., Verheggen, T. P., Mikkers, F. E., *J. Chromatogr.* 1979, *169*, 21–38.

[15] Dolnik, V., Deml, M., Bocek, P., *J. Chromatogr.*1985, *320*, 89–97.

[16] Bodor, R., Madajova, V., Kaniansky, D., Masar, M., Johnck, M., Stanislawski, B., *J. Chrom. A* 2001, *916*, 155–165.

[17] Kaigala, G., Behnam, M., Bliss, C., Khorasani, M., Ho, S., McMullin, J., Elliott, D., Backhouse, C., *IET Nanobiotechnol.* 2009, *3*, 1–7.

[18] Everaerts, F. M., Beckers, J. L., Verheggen, Th. P. E. M., *Isotachophoresis-Theory, Instrumentation and Applications*, Elsevier, Amsterdam 1976.

[19] Kohlrausch, F., *Ann. Phys. Chem.* 1897, *298*, 209–239.

[20] Alberty, R. A., *J. Am. Chem. Soc.* 1950, *72*, 2361–2367.

[21] Jovin, T. M., *Biochemistry* 1973, *12*, 871–879.

[22] Jung, B., Bharadwaj, R., Santiago, J. G., *Anal. Chem.* 2006, *78*, 2319–2327.

[23] Saville, D. A., Palusinski, O. A., *AIChE J.* 1986, *32*, 207–214.

[24] Hruška, V., Jaroš, M., Gaš, B., *Electrophoresis* 2006, *27*, 984–991.

[25] Bercovici, M., Lele, S. K., Santiago, J. G., *J. Chromatogr. A* 2009, *1216*, 1008–1018.

[26] Bercovici, M., Lele, S. K., Santiago, J. G., *J. Chromatogr. A* 2010, *1217*, 588–599.

[27] Hruška, V., Gaš, B., Vigh, G., *Electrophoresis* 2009, *30*, 433–443.

[28] Zhukov, M. Yu., *Comput. Math. Math. Phys.* 1984, *24*, 138–149.

[29] Zusková, I., Gaš, B, Vacík, J., *J. Chromatogr.* 1993, *648*, 233–244.

[30] LeVeque, R. L., *Finite Volume Methods for Hyperbolic Problems*, Cambridge University Press, Cambridge, UK 2002.

[31] Persat, A., Suss, M. E., Santiago, J. G., *Lab Chip* 2009, *9*, 2454–2469.

[32] Ghosal, S., *Annu. Rev. Fluid Mech.* 2006, *38*, 309–338.

[33] Bhardwaj, R., Santiago J. G., *J. Fluid Mech.* 2005, *543*, 57–92.

[34] Khurana, T. K., Santiago, J. G., *Lab Chip* 2009, *9*, 1377–1384.

[35] Hirokawa, T., Taka, T., Yokota, Y., Kiso, Y., *J. Chromatogr.* 1991, *555*, 247–253.